EurJIC
European Journal of Inorganic Chemistry

Full Papers
doi.org/10.1002/ejic.202001174

Chemistry Europe
European Chemical Societies Publishing

Biotin-Appended Iron(III) Complexes of Curcumin for Targeted Photo-Chemotherapy

Somarupa Sahoo,[a] Abinaya Raghavan,[b] Arun Kumar,[a] Dipankar Nandi,*[b] and Akhil R. Chakravarty*[a]

Iron(III) complexes of curcumin (Hcur) having a tridentate *NNN*-donor dipicolylamine-based ligand L^1 and its biotinylated analogue L^2, namely, [Fe(L^1)(cur)Cl] (**1**) and [Fe(L^2)(cur)Cl] (**2**), were prepared, characterized and their photo-induced cytotoxicity studied. The complexes exhibited curcumin-based absorption band near 430 nm and emission maxima at 520 nm. Complex **2** with a biotin moiety showed enhanced cellular uptake and higher cytotoxicity compared to its non-biotin analogue **1**. The visible light induced cytotoxicity was studied in HeLa, MCF-7 and HepG2 cell lines. Complex **2** displayed photodynamic effect (400–700 nm, 10 J cm^{-2}) giving an IC_{50} value of ~4 μM in HeLa and MCF-7 cells, while being significantly non-toxic in the dark ($IC_{50} > 100$ μM). A 5-fold increase in cytotoxicity was observed in HepG2 cells (IC_{50} ~0.7 μM) for the biotin-appended complex **2**. In vitro generation of reactive oxygen species (ROS) was observed from dichlorofluorescein diacetate (DCFDA) assay. The mode of cell death was apoptotic. Formation of hydroxyl radicals as the ROS was evidenced from the plasmid pUC19 DNA photo-cleavage studies. The complexes demonstrated the ability to act as targeted PDT (photodynamic therapy) drugs.

Introduction

Cancer, being one of the leading causes of human death, has attracted attention to develop the chemistry of new generation chemotherapeutic drugs.[1,2] Available chemotherapeutics suffer from various limitations as these cytotoxins do not distinguish between cancer versus normal cells thus leading to undesirable side-effects.[3] In addition, the nuclear DNA targeting drugs suffer from dose limitations that arise from the nuclear excision repair (NER) mechanism operating inside the cell nucleus.[4,5] Photodynamic therapy (PDT), which is based on selective activation of a photosensitizer in tumor by laser of suitable wavelength, has emerged as a viable alternative methodology for cancer cure and management.[6–10] The currently used PDT drug is Photofrin® which shows variable side-effects such as skin irritation due to distribution of the drug throughout the body, and hepatic disorder (jaundice) due to formation of bilirubin on heme degradation.[11,12] To overcome such drug reactions, systematic efforts are on to develop new generation tumor-specific delivery systems for chemotherapeutic as well as PDT action. In the recent times, transition metal complexes have received a lot of attention as they offer rich photophysical and tunable redox properties along with their amenable coordination geometry. This helps in modelling metallo-drugs of multiple functionalities for targeted photo-chemotherapy.[13–15] The efficacy of the drugs can be enhanced significantly by recognizing the intrinsic differences between the normal and tumor cells.

As rapidly dividing cancer cells require enormous number of vital biomolecules to sustain their rapid division, many tumor specific receptors are overexpressed in such cells. These receptors have been used as targets to deliver toxic agents into the tumors.[16] Vitamin receptors in cancer cells fall under this category. Therefore, vitamin receptors serve as useful biomarkers for tumor targeted drug delivery.[17–19] Vitamin B12, folic acid, biotin and riboflavin are essential components for the synthesis of DNA nucleobases. The folate receptors have been well studied for targeted drug delivery. Biotin (also called as Vitamin H or Vitamin B7), which is a growth promoter at cellular level has the potential for such highly targeted drug delivery applications. Biotin has been established to have a strong binding affinity for protein receptors like avidin and streptavidin (~10^{14} M).[20] The present work stems from our continued interest towards designing mixed-ligand iron(III) based anti-cancer agents for cancer cell targeting and apoptotic cell death.[21–24] Recent studies have indicated that curcumin can modulate different biological processes involved in cell cycle regulation, mutagenesis, tumorigenesis and apoptosis. It has also been revealed in *in vitro* studies that the mitochondria-mediated pathway of apoptosis involving caspases and Bcl-2 family of proteins can be induced by curcumin.[25] We have recently reviewed the current status of the chemistry of metal curcumin complexes and the in vitro photo-induced cytotoxicity observed in such species.[26] Curcumin as such, however, is not suitable for therapeutic action because of its rapid degradation in a biological medium resulting in severe

[a] S. Sahoo, Dr. A. Kumar, Prof. Dr. A. R. Chakravarty
Department of Inorganic and Physical Chemistry
Indian Institute of Science,
Bangalore 560012, Karnataka, India
E-mail: arc@iisc.ac.in
http://ipc.iisc.ac.in/~arc/
[b] A. Raghavan, Prof. Dr. D. Nandi
Department of Biochemistry
Indian Institute of Science
Bangalore 560012, Karnataka, India
E-mail: nandi@iisc.ac.in
http://biochem.iisc.ernet.in/dpnLab/

Supporting information for this article is available on the WWW under https://doi.org/10.1002/ejic.202001174

limitations like poor bioavailability and reduced efficacy.[27] This degradation can be arrested in a significant manner upon its binding to iron(III).[28–30] We have thus chosen curcumin as a ligand in the mixed-ligand complex structure because of its profound medicinal values and ROS generating properties upon photo-excitation, while biotin is chosen as the vitamin for its cell targeting property.[31–33] We could also use the green emission of curcumin for cellular imaging and to study the cellular uptake of the complexes via fluorescence-activated cell sorting (FACS).[34] Fe-bleomycins were one of the earliest and extensively used agents for DNA damage.[35] Following the FDA approval, they were used for treating Hodgkin's lymphoma and testicular cancer. That has led to a lot of interest in Fe-based anti-cancer agents.[35] We were keen to explore the photo-chemotherapeutic action of photosensitizers coordinated to an Fe(III) core. Iron being a bio-available metal reduces the systemic toxicity associated with heavy metal-based photo-sensitizers. Iron(III) complexes having curcumin and the biotinylated dipicolylamine ligands are thus designed and synthesized to achieve ROS (reactive oxygen species) mediated photo-induced cytotoxicity.

Herein, we report the synthesis and anticancer activity of two iron(III) complexes of curcumin (Hcur), namely, [Fe(L)(cur)Cl]Cl, where L is ethylenediamine-N,N-bis((pyridin-2-yl)methyl)-methanamine in **1** and biotin appended dipicolylamine in **2** (Figure 1). Internalization of the curcumin complexes inside the cells was studied and cellular uptake was assessed by monitoring the curcumin-based fluorescence of the complexes. The significant results of this work include the hydroxyl radical mediated photocytotoxic effect of the complexes in broad band visible light (400–700 nm) and selective uptake of the biotin complex **2** in HepG2 cancer cells.

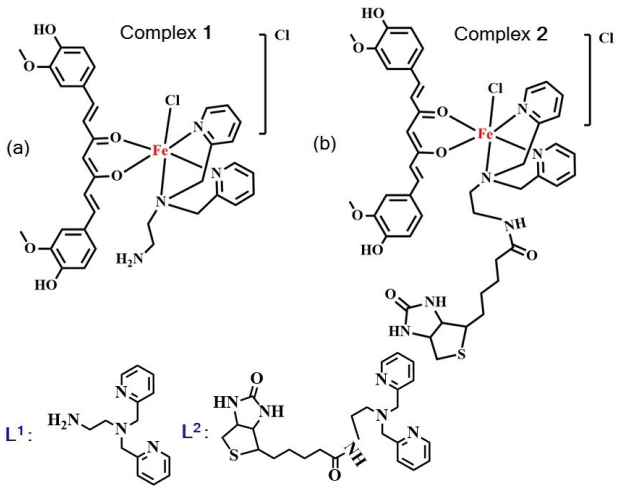

Figure 1. Schematic drawings of ligands L^1 and L^2 along with iron(III) complexes **1** and **2** as their chloride salts.

Results and Discussion

Synthesis and General Properties

The *N*,*N*-bis((pyridin-2-yl)methyl)methanamine (dipicolylamine) based ligands L^1 and L^2 were synthesized. The synthesis of biotin-conjugated dipicolylamine (DPA) L^2 was carried out using a protocol given in Scheme S1 (vide Supporting Information). This ligand was characterized by basic techniques (Figures S1-S3, S5). Complex **1** has L^1 (ethylenediamine-DPA) and curcumin as the ligands, whereas complex **2** has a biotin-DPA conjugate (L^2) and curcumin in its monoanionic form. Complex **1** was used as a control to study the effect of free amine group on the cellular uptake of the complexes. As biotin receptors are overexpressed in many cancer cell lines, complex **2** with an appended biotin unit was prepared to achieve enhanced cellular uptake. Curcumin, which is known to be an effective anti-tumor agent, was incorporated in the structure as a photosensitizer. The choice of a tridentate *NNN*-donor and a β diketonate *OO*-donor ligand in the mixed-ligand complexes is to stabilize the iron(III) redox state in the cellular medium where intracellular reducing agents like thiols are present. The iron(III) complexes [Fe(L)(cur)Cl]Cl were prepared in good yields by first reacting anhydrous $FeCl_3$ with L^1 or L^2, isolating the intermediate $Fe(L^1/L^2)Cl_3$ and then with a methanol solution of curcumin (Hcur) that was previously deprotonated with triethylamine (Scheme S2). The products were isolated as deep brown colored solid. The complexes were characterized from various physico-chemical parameters (Figures S4-S6). Selected physicochemical data are presented in Table 1. The ESI-mass spectra of the complexes showed a single peak corresponding to the $[M-Cl]^+$ in CH_3CN at 700.2156 and 926.2710 for complexes **1** and **2** respectively (Figures S4, S5).

Photo-physical and Photochemical Study

The complexes had good solubility in methanol, dimethyl sulfoxide (DMSO), and dimethylformamide (DMF). They were also soluble in 20% DMSO/DPBS (Dulbecco's phosphate-

Table 1. Selected physicochemical and ct-DNA binding data of the complexes **1** and **2** as their chloride salts.

Complex	Λ[nm] [ε/M^{-1} cm^{-1}}[a]	λ_{em}[b] [nm] (Φ_F)	Λ_M[c] [$S cm^2 M^{-1}$]	E_{pc}[d] [V]	K_b[e] [M^{-1}] [s]	μ_{eff}[f]/μ_B
1	437 (32500)	518 (0.03)	58	−0.47	7.8×10^5 (±0.2)	5.83
2	440 (30700)	521 (0.05)	63	−0.51	6.3×10^5 (±0.3)	5.87

[a] In 1:1 DMF/DPBS buffer (pH 7.2, 25 °C). [b] In DMSO; λ_{ex} = 430 nm (fluorescence quantum yield with respect to fluorescein with Φ_F = 0.79 in 0.1 M NaOH). [c] Molar conductivity value in DMF at 25 °C. [d] Cathodic peak potential vs. SCE in 5 mL DMF with 0.1 M TBAP at a scan rate of 50 $mV s^{-1}$; ferrocene was used as a standard. [e] Intrinsic binding constant to ct-DNA (s, MvH eq. fitting parameter). [f] $Hg[Co(SCN)_4]$ used as standard.

buffered saline). This is important as curcumin (Hcur) itself is sparingly soluble in the biological medium. The enhanced solubility of curcumin in metal-bound form is expected to increase its uptake into the tumor site. They were insoluble in hydrocarbons like hexane, toluene and benzene. The IR spectra of the complexes showed two characteristic strong intensity bands around 1585 and 1490 cm^{-1} for the C=O and C=C (β-diketonate) stretching vibrations, respectively.[36] There was a blue shift from the same bands of free curcumin (1607 and 1510 cm^{-1} respectively). This suggested binding of curcumin in its enolate form to iron(III) in a bidentate fashion (Figure S7).[37] Cyclic voltammetry of the complexes showed their redox activity. A quasi-reversible Fe^{III}–Fe^{II} redox couple was observed near –0.5 V (ΔE_p = 80–90 mV at 50 mV s^{-1}) versus SCE (saturated calomel electrode) in DMF (5 mL)-TBAP (0.1 M; tetrabutylammonium perchlorate as supporting electrolyte). However, there was no oxidative response in the complexes in anodic scans suggesting the redox stability of Fe(III) (Figures S8, S9).

Since the redox potential for Fe^{III}/Fe^{II} is beyond the biological window, the complexes are unlikely to get reduced in the presence of cellular thiols thus eliminating any possibility of their chemical nuclease activity.[38] This is expected to reduce any dark cytotoxicity in the cell proliferation assays. The iron(III) complexes behaved as 1:1 electrolytes with respective molar conductance value of 58 and 63 S m^2 M^{-1} in DMF at 25 °C. The data indicate the non-dissociable nature of the metal-bound chloride ligand. Magnetic susceptibility measurements on the complexes at 25 °C gave magnetic moment values of 5.83 and 5.87 μB, indicating high spin ($t_{2g}^3 e_g^2$) configuration of the $3d^5$ iron(III) centers in pseudo-octahedral coordination geometry.

The electronic absorption spectra of the complexes in 1:1 (v/v) DMSO/DPBS showed an intense visible band at 440 nm with a shoulder at around 454 nm. This is for π to π* transition emerging from the curcumin ligand (Figure 2).[39]

In addition, low energy ligand π to metal dπ charge transfer (CT) electronic transition was observed near 440 nm. This band was used to explore the photo-induced DNA cleavage activity of the complexes in Tris-HCl/NaCl (50 mM) buffer (pH 7.2). The photo-stability of the complexes was monitored for up to 48 h by absorption spectroscopy in 20% DMSO/DPBS medium with 1 h photo exposure time (broadband visible light source of 400–700 nm) (Figures S10-S12). It can be seen from the plots that curcumin ligand alone degrades extensively within 4 h (Figure 3a). In contrast, the band intensities of the complexes were relatively stable up to 12 h which is well over the experimental cell incubation time of 4 h. The time dependent absorption spectra of the complexes and HCur shown in Figure S10 (vide Supporting Information) highlight the high stability of curcumin in its metal-bound form. Stability of the complexes was also studied in presence of biological reducing agent glutathione (GSH) (Figure 3b). The fluorescence intensity of the complexes was monitored over a 60 min period. There was a very small change in the emission values indicating negligible displacement of curcumin from the iron core. The observed minimal changes in the absorption spectra suggested the stability of the complexes even after 1 h photo-irradiation, thus making them suitable for cellular studies.

Complexes **1** and **2** showed an emission band near 535 nm in 10% aqueous DMSO giving fluorescence quantum yield (ϕ) values of 0.03 and 0.05 respectively (Figure 2, Table 1). The curcumin ligand alone is known to give a ϕ value of 0.042 under similar experimental conditions.[39] This suggests that the fluorescence resulting from the curcumin ligand is retained in the iron(III) complexes indicating no apparent leaching of the metal from the complex in solution. The complexes are thus suitable for *in-vitro* localization study by confocal imaging. The energy-optimized structures of the complexes were obtained by density functional theory (DFT), using B3LYP with the LanL2DZ basis set for all atoms, with the Gaussian 09 software package.[40] For both the complexes the HOMO lies on the curcumin unit whereas LUMO resides on the dipicolylamine moiety (Figure 4).

The energy difference between LUMO and HOMO for the complexes is ~2.5 eV (Tables S1, S2). The weak band at 600 nm is attributed to the excited state 9 which is arising because of the transition between HOMO 218(B) to LUMO 226(B). The weakness of this transition is because of low transition probability of 34%.

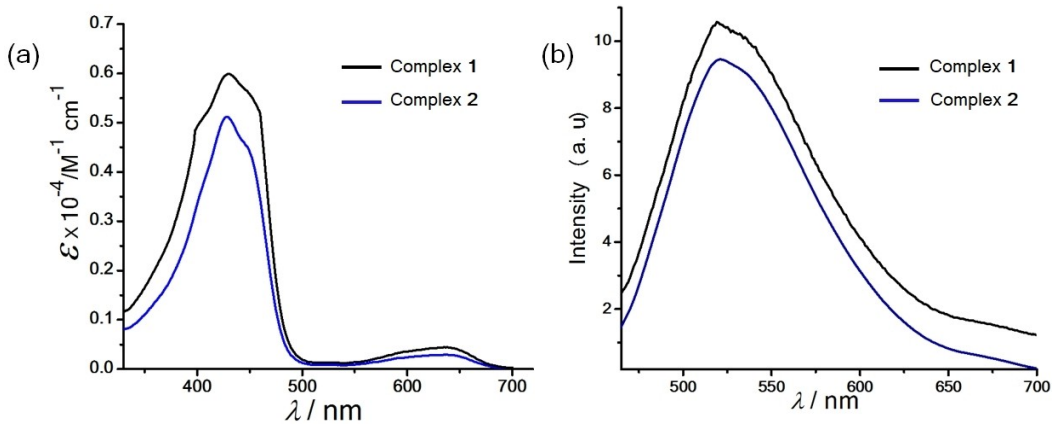

Figure 2. (a) Absorption spectra of the complexes **1** (black) and **2** (blue) in 1:1 (v/v) DMSO/ DPBS buffer medium. (b) Emission spectra of the complexes **1** and **2** in 20% aqueous DMSO (λ_{ex}: 430 nm).

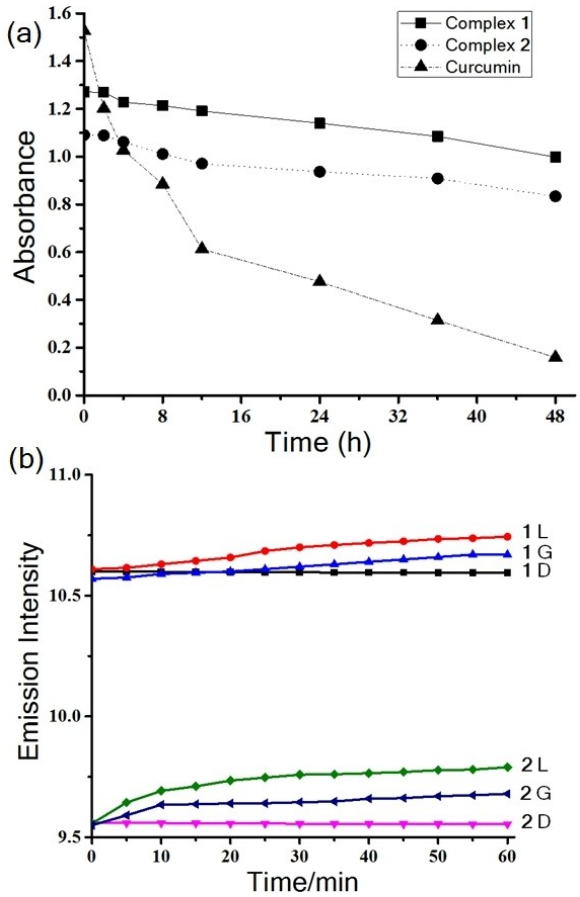

Figure 3. (a) Photo-stability of the complexes and curcumin studied up to 48 h in 1:1 DMSO/DPBS medium upon 1 h irradiation with visible light (400–700 nm). (b) Fluorescence intensities of the complexes (20 μM in DMSO) in the dark (D), in visible light of 400–700 nm (L, 10 J cm^{-2}), and with one eq. of glutathione (G) for a period of 1 h.

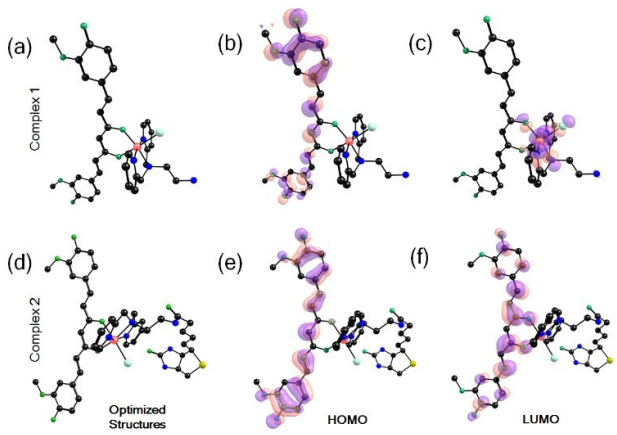

Figure 4. (a, d) Geometrically optimized structures of the complexes **1** and **2** obtained from DFT calculations using B3LYP level and LanL2DZ basis set. (b, c, e, f) Frontier molecular orbitals (HOMO, LUMO) of the complexes.

Cytotoxicity and Cellular Uptake

To assess the ability of the complexes **1** and **2** to induce photo-activated cell death in visible-light (400–700 nm; Luzchem photoreactor, 10 J cm^{-2}; irradiation time of 1 h), a cell viability MTT assay was performed using HeLa (human cervical cancer cell line), MCF-7 (human breast cancer cell line), and HepG2 (human liver cancer cell line) (Table 2, Figure 5, Figures S13-S15). HeLa cells were used as a fast-growing human cell line model, whereas MCF-7 is a slightly slower growing breast cancer cell line model system.

Since it is known that liver cancer cells have an increased number of nutrient receptors on the cell surface that are avid binders to biotin, HepG2 cells were used to study the effect of differential uptake of the drug in the dosage required to inhibit 50% of cell proliferation (IC_{50}). A significant dose dependent cytotoxic activity was observed in all the cell lines upon photo-irradiation with visible light after treatment with the complexes. Both the complexes remained essentially non-cytotoxic in the dark (IC_{50}: >100 μM), while the IC_{50} values for complex **1** were in the range of 6–7 μM in all the cell lines. The low IC_{50} values indicated that the presence of free NH_2 moiety helps in the cellular uptake of the complexes. The IC_{50} values were found to be lower (~4 μM) in HeLa and MCF-7 upon treatment with the biotinylated complex **2**. This could be due to an enhanced uptake via receptor mediated endocytosis for complex **2** having the conjugated biotin moiety. The IC_{50} value of complex **2** for HepG2 cells decreased significantly to 0.74 μM. The IC_{50} data emphasize the role of biotin receptors on the surface of these cells. To ascertain the role of receptors, this assay was performed using HepG2 cells that were pre-saturated with 2 mM biotin for 1 h, so that the receptor channels were blocked by the externally added biotin. It was observed that the IC_{50} value increased to 12.2 μM, thus indicating that the uptake of the complexes was mediated by cell surface receptors (Fig-

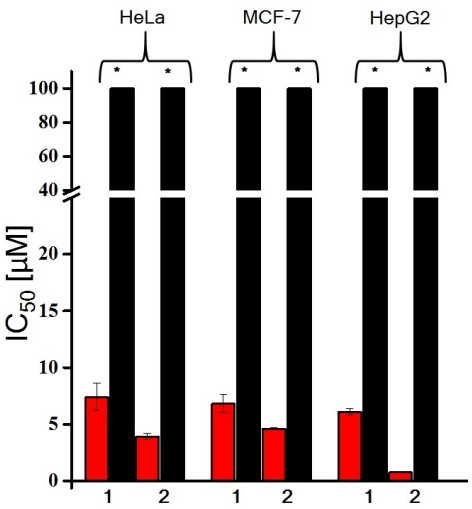

Figure 5. Bar diagram showing cytotoxicity of the complexes **1** and **2** in cancer cell lines, viz. HeLa, MCF-7 and HepG2. Light source: 400–700 nm, 10 J cm^{-2}, 1 h (>100 μM indicates no dark toxicity up to the concentration used. Left bar is in light and the right one for dark).

Table 2. The IC_{50} values (μM) of the complexes **1** and **2** in HeLa, MCF-7 and HepG2 cells with other relavant compounds[a]

Compound/Cells	HeLa Light[b]	HeLa Dark	MCF-7 Light[b]	MCF-7 Dark	HepG2 Light[b]	HepG2 Dark	Fe content[a]
1	7.4 (±1.2)	>100	6.8 (±0.8)	>100	6.1 (±0.3)	>100	155 (±3)
2	3.9 (±0.3)	>100	4.6 (±0.1)	>100	0.74 (±0.04)	>100	223 (±5)
Curcumin	8.2 (±0.2)	85.0 (±4)[c]	19.9 (±1.4)[d]	90.3 (±4.9)[d]	17.5 (±3.2)[e]		
Cisplatin[f]	–	10.5 (±2.9)	-	2.0 (±0.3)[f]	92 (±4.6)		
[VO(TPPphtpy)-(cur)](ClO_4)[g]	6.7 (±0.6)	17.9 (±1.6)	6.7 (±1.5)	22.4 (±2.1)	–	–	
[Cu(L^2)(cur)]Cl[h]	3.8 (±0.2)	32.1 (±0.4)	–	–	–	–	
Photofrin®[i]	4.3 (±0.2)	>41	–	–			
[{Fe(L)(cur)}$_2$ (μ-O)]$(ClO_4)_2$ [j]	3.1 (±0.4)	>50	4.9 (±0.5)	90.3 (±4.9)			

[a] The estimated deviations in the IC_{50} values are given in the parenthesis. Intracellular Fe estimation by ICPMS using standards for calibration, expressed in (ng/10^6 HeLa cells). [b] The IC_{50} values correspond to 4 h incubation in dark followed by photo-exposure for 1 h to visible light of 400–700 nm (10 J cm^{-2}). [c] Data from reference [41]. [d] Values are from reference [42]. [e] IC_{50} value corresponds to 24 h incubation in the dark. The values for 96 h treatment are taken from reference [43]. [g] Values are from reference [27]. [h] L^2 is a diiodinated BODIPY ligand; Values are from reference [38]. [i] The values are taken from reference [44] and are converted to μM using the approximate molecular mass of Photofrin® (600 g mol^{-1}) with 633 nm excitation with a fluence rate of 5 J cm^{-2}. [j] L is bis-(2-pyridylmethyl)-benzylamine. Values are from reference [45].

ure S15c). To further elucidate the role of the ligands on the cytotoxicity, MTT assay was performed in HeLa cells using the ligands alone as a control. It was observed that both the ligands remained non-toxic up to 200 μM in light and dark conditions. The IC_{50} values of the present complexes along with selected curcumin metal complexes, cisplatin and Photofrin® are listed in Table 2.[41–45] The PDT effect of complexes **1** and **2** compares well with that of the PDT drug Photofrin®.

To investigate whether the biotin moiety possessed any selective role in facilitating the uptake of the complexes into the cancer cells, flow-cytometry-based cellular-incorporation assays were performed. It was observed that the uptake of complex **2** was much higher than complex **1** after 4 h of incubation in HeLa cells (Figure 6).

This suggests higher uptake of complex **2** in the cells, possibly due to increased demand for biotin as a nutrient. In addition to that, an increase in the uptake of this complex into the cells was observed with an increase in the incubation time. Notably, complete incorporation into HeLa cells was found at 4 h post-incubation time (Figure S16). This incubation time was thus used for all other in vitro studies. Furthermore, it was observed that the uptake of complex **2** into the HeLa cells decreased upon pre-saturating the cells with external biotin (2 mM) (Figures S15(c), S17). This could be attributed to selective uptake of the complex by biotin transporter channels initially, which gives way to internalization by simple diffusion pathway with the passage of time. This uptake trend was further verified by ICPMS (Inductively Coupled Plasma Mass Spectroscopy) assay where it was observed that concentration of iron inside the HeLa cells increased from 74 ng/10^6 cells to 155 ng/10^6 cells upon incubation with complex **1**, while the concentration increased ~3 times (223 ng/10^6 cells) in the case of complex **2**. This observation further strengthens the argu-

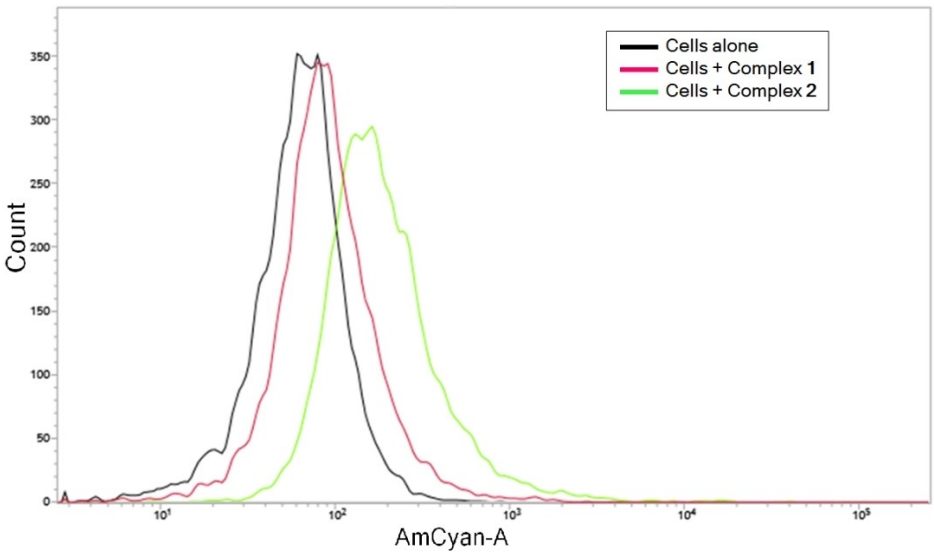

Figure 6. Histogram showing cellular incorporation of complex **1** (red line) and complex **2** (green line) in HeLa cells post 4 h of incubation at 37 °C. Complex concentration: 2 μM.

ment that the appended biotin moiety enhanced the internalization of the complex.

Annexin V-FITC-PI Assay

Annexin V-FITC (fluorescein isothiocyanate)/PI (propidium iodide) assay was performed in HeLa cells and the results were analyzed by fluorescence assisted cell sorting (FACS) analysis in order to assess the ability of the complexes to induce apoptotic (programmed) cell death upon light irradiation. This assay was used to get an estimate of the apoptotic cells: early – high annexin V-FITC and low PI (Q4), viable cell – unstained, only showing auto-fluorescence (Q3), late – high annexin V-FITC and PI (Q2) and necrotic cell populations – stained with PI only (Q1); Q stands for quadrant.[46]

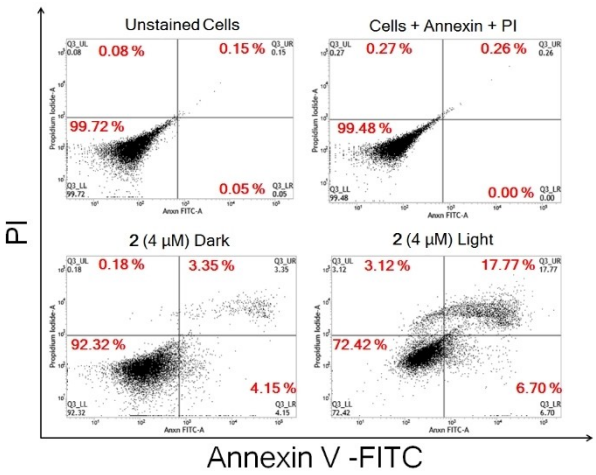

Figure 7. Annexin-V–FITC–PI assay showing the percentage population of early apoptotic cells stained by annexin-V–FITC alone (lower right quadrant), dead cells stained by propidium iodide (PI) alone (upper left quadrant), and late apoptotic cells stained by both annexin-V–FITC and PI (upper right quadrant), in HeLa cells alone and treated with complex **2** (4 μM), in the dark or after exposure to visible light for 1 h (400– 700 nm).

The cells, pretreated with 4 μM of complex **2**, were stained with Annexin-V FITC and PI and then studied in dark and after photo irradiation. The percentage of cell population in these four stages upon treatment of the cells with complex **2** are indicated in the plots shown in Figure 7. From the dot plots, an increase in the cell population in the quadrant Q4 is evidenced. We can thus infer that the complexes are capable of inducing apoptosis.

Complex **2** induced about 25 % apoptosis in 4 μM concentration upon 1 h photo irradiation with visible light (400–700 nm). The population of cells in necrosis mode (stained with PI) is significantly lower, which suggests the overall apoptotic mode of cell death. The complex in dark failed to cause any apoptosis, which also explains the excellent cell viabilities in dark upon treatment with the complexes as seen from the MTT assay.

As the complexes induced apoptotic cell death in a dose dependent manner, the source of cytotoxicity was investigated. Curcumin is known to produce hydroxyl radicals as the reactive oxygen species (ROS) upon photo-activation. To ascertain the *in vitro* ROS formation, complex **2** was probed by DCFDA (2′,7′ dichlorofluorescein diacetate) assay in HeLa cells on exposure to light (400–700 nm) at its IC_{50} concentration (Figure 8).[47] The cell permeable DCFDA upon oxidation by ROS generates green fluorescent DCF, which shows an emission maximum at 528 nm.

That can be readily detected and quantified by FACS method. The shift in the band position can be correlated with the amount of ROS generated within the cell. After incubating for 4 h in the dark, the band for DCFDA coincided with that of the control (cells + DCFDA). This means there was no apparent generation of ROS (Figure 8). However, upon photo-exposure to visible light for 1 h, a bathochromic shift in the band position was observed. This assay clearly suggests generation of ROS

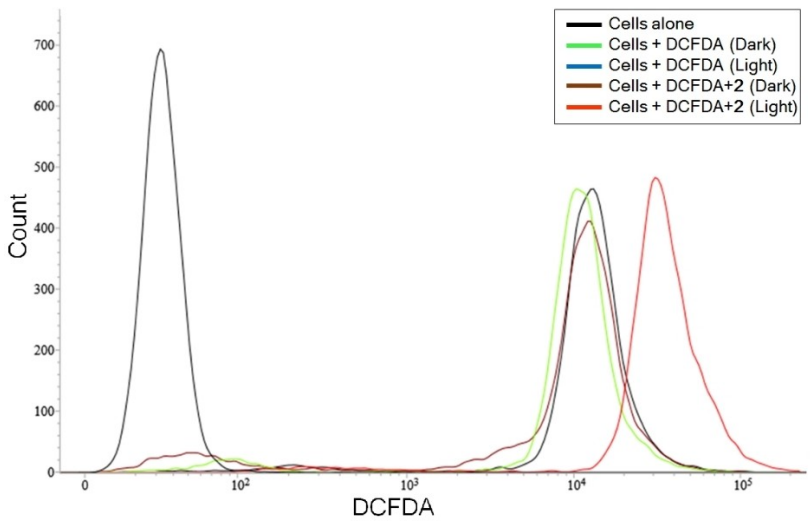

Figure 8. Flow-cytometric analysis showing ROS generation by complex **2** in the dark and upon irradiation with visible-light in HeLa cells. The greater positive shift in the fluorescence of DCF (red line) indicates the greater extent of ROS generation in visible light (400–700 nm).

only upon photo-irradiation of the curcumin complexes in visible light.

Cellular Localization

The intracellular localization of the green-emissive complex **2**(20 μM) was monitored by confocal microscopy. In each case, green fluorescence was observed predominantly in the cytoplasm with negligible nuclear uptake (Figure 9). The cells were also stained with Hoechst, Mito-Tracker deep red (MTR) and Lyso-Tracker deep red (LTR) to study the subcellular localizations. While there was no overlap with the Hoechst, the complex gave a PCC (Pearson correlation coefficient) of ~0.4 with both MTR and LTR (Figures S18, S19) indicating that the complex localizes primarily in the cytosol.

DNA Binding and Cleavage Studies

The anti-proliferative and apoptosis inducing properties of the complexes prompted us to study their interaction with the DNA. The intrinsic DNA binding constant (K_b) values of the complexes were determined from the absorption spectral traces of complexes **1** and **2** in Tris–HCl buffer (5 mM; pH 7.2) by increasing the quantity of calf thymus (ct) DNA while keeping the complex concentration as constant (Figure S20).[48] The K_b values of complexes **1** and **2** were in the range of ~10^5 M^{-1} suggesting partial intercalative mode of DNA binding. The binding strength is in the order: **1** < **2**. The DNA cleavage activity of complexes (25 μM) was studied using supercoiled pUC19 DNA (30 μM, 0.2 μg) in Tris-HCl/NaCl (50 mM) buffer (pH 7.2) to explore the nature of the ROS. Monochromatic visible light source of 446 nm (50 mW power) was used from a continuous-wave (CW) diode laser for irradiation. The wavelength was chosen based on the visible absorption band of curcumin and the LMCT band. Both the complexes produced no apparent cleavage of supercoiled (SC) DNA in the dark. Upon photo exposure of 1 h, the %NC (nicked circular) DNA was found to be ~96% (Figure S18). Control experiments using ligands L^1 and L^2 showed no apparent DNA photo-cleavage activity in visible light. The "chemical nuclease" activity of the complexes was explored in the presence of glutathione (GSH) as a reducing agent and H_2O_2 as an oxidizing agent (Figure S19). About 6% of NC DNA was formed in the presence of GSH indicating the redox stability of the complexes towards reduction of iron(III) by cellular thiols. The %NC DNA increased to ~13% in the presence of H_2O_2 which may be due to catalytic decomposition of hydrogen peroxide by iron(III), forming radical species.[49]

The ROS could be radical species or singlet oxygen based on type-I or type-II pathway. To ascertain this, pUC-19 DNA was treated with the complexes and photo-exposed in the presence of various additives (Figure 10, Figures S18-S20).[50] The complexes showed ~15% NC DNA under an argon indicating the necessity of molecular oxygen ($^3O_2$) to observe the DNA photocleavage activity. The reactions under aerobic conditions could proceed via two major mechanistic pathways. The excited electronic state of the complex through efficient intersystem crossing could generate excited triplet state that can activate $^3O_2$ to the reactive singlet oxygen ($^1O_2$) by a type-II process. In an alternate pathway, the photo-activated complex could reduce molecular oxygen to generate reactive hydroxyl radical

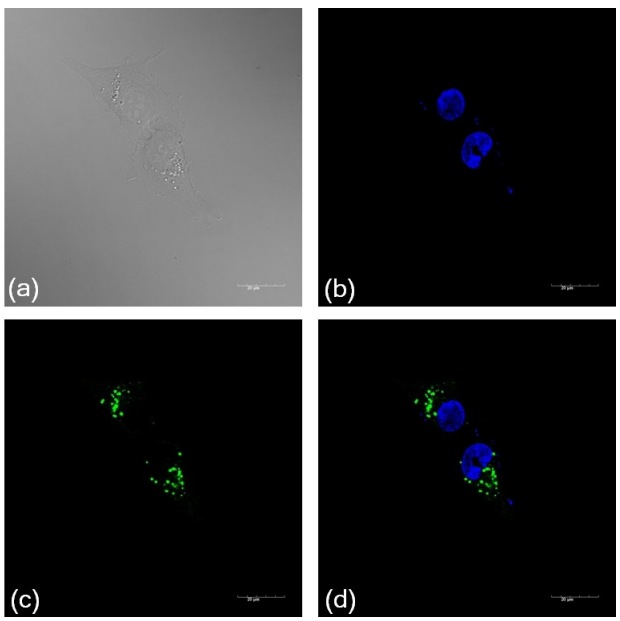

Figure 9. Confocal microscopic images of HeLa cells after 4 h incubation with complex **2**: panel (a) is bright field; panel (b) is for the fluorescence of Hoechst dye which localises in the cell nucleus; panel (c) is for the fluorescence of complex **2**; panel (d) shows the merged image of (b) and (c) (Scale bar = 20 μm, magnification 100X).

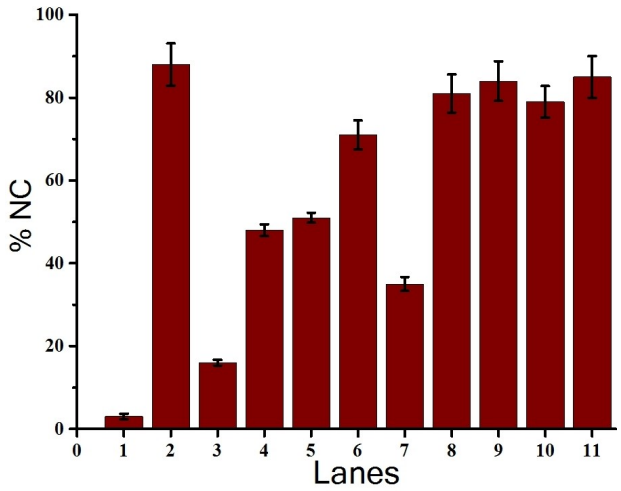

Figure 10. (a) Bar diagram showing the mechanistic aspects of photo nuclease activity of complex **2** (25 μM), in the presence of various singlet oxygen quenchers and radical scavengers on 1 h irradiation with 446 nm (75 mW power) continuous-wave (CW) diode laser (L): Lane 1: pUC19 DNA alone; lane 2: DNA + **2** (Light, L); lane 3: DNA + **2** under Argon (L); lane 4: DNA + **2** + KI (0.5 mM) (L); lane 5: DNA + **2** + DMSO (4 μL, L); lane 6: DNA + **2** + SOD (superoxide dismutase, 4 units, L); lane 7: DNA + **2** + catalase (4 units, L); lane 8: DNA + **2** + TEMP (0.5 mM, L); lane 9: DNA + **2** + NaN_3 (0.5 mM, L); lane 10: DNA + **2** + DABCO (0.5 mM, L); lane 11: DNA + **2** + D_2O (16 μL, L).

(HO•) by a photo-redox mechanism.[51] The mechanistic aspects of the plasmid pUC19 DNA photo-cleavage reactions were studied in the presence of singlet-oxygen quenchers, namely, DABCO (1,4-diazabicyclo[2.2.2]octane), NaN_3, and TEMP (2,2,6,6-tetramethylpiperidine); hydroxyl radical scavengers, namely, KI and DMSO; catalase as a H_2O_2 scavenger; and superoxide dismutase (SOD) as a superoxide radical scavenger. Singlet oxygen quenchers did not show any inhibitory effect as the % NC remained at ~80%, thus eliminating the possibility of $^1O_2$ (singlet oxygen) formation. However, in the presence of KI, DMSO and catalase, as hydroxyl radical scavengers, a significant decrease in the DNA photo-cleavage activity (~35%) was observed. The results indicate formation of hydroxyl radical (•OH) as the ROS in a photo-redox pathway following a mechanism which could be similar to that of photo-Fenton process ($UV/Fe^{2+}/H_2O_2$).[52] The full gel diagrams of this study are given in Figures S21-S23 (vide Supporting Information).

Conclusions

Mixed-ligand iron(III) complexes having cell-targeting biotin moiety and photosensitizing curcumin unit were designed and studied for their targeted photo-cytotoxicity in visible light. The complexes showed higher incorporation into the liver cancer cells and exhibited excellent photo-cytotoxicity in visible light (400 − 700 nm), while remaining essentially non-toxic in the dark. The complexes as avid binders to ct-DNA showed hydroxyl radical mediated plasmid DNA cleavage activity with no apparent chemical nuclease activity. The complexes displayed significant arrest of degradation of curcumin on binding to Fe(III) and no apparent leaching of the metal in the experimental conditions thus indicating their photo-stability over a period of 48 h. The complexes exhibited remarkable photo-induced toxicity in the cancer cells. In addition, the biotinylated complex 2 displayed a 5-fold decrease in the IC_{50} values in HepG2 cancer cells at sub-micromolar IC_{50} concentration. Annexin-V assay revealed the apoptotic mode of cell death induced by ROS generated by the complexes on visible light irradiation. The results highlight the significant therapeutic potential of the iron-based photo-chemotherapeutic agents.

Experimental Section

Materials and Methods

The reagents and chemicals were procured from the commercial sources (s. d. Fine Chemicals, India; Sigma-Aldrich, U.S.A., E-Merck and Alfa Aesar, U.K.). Synthesis of the complexes was performed under nitrogen atmosphere using Schlenk technique. Supercoiled (SC) pUC19 DNA (cesium chloride purified) was from Bangalore Genie (India). Solvents used were purified and distilled by standard methods.[53] Tris(hydroxymethyl)aminomethane-HCl (Tris-HCl) buffer (pH = 7.2) was prepared using deionized and sonicated double distilled water. Dulbecco's Modified Eagle's medium (DMEM), 3-(4,5-dimethylthiazol-2-yl)-2,5-diphenyltetrazolium bromide (MTT), 2,7-dichlorofluorescein diacetate (DCFDA), calf thymus (ct) DNA, agarose (molecular biology grade), 2,2,6,6-tetramethyl-4-piperidone (TEMP), ethidium bromide (EB), 2-picolylamine and curcumin (HCur) were purchased from Sigma–Aldrich (U. S. A.) and used as received. Annexin-V/PI kit was procured from Thermo-Fisher. Tetrabutylammonium perchlorate (TBAP) was prepared by reacting tetrabutylammonium bromide and perchloric acid. It was used in small quantity with great care (*caution!*). Mito tracker deep red (MTR) and fetal bovine serum (FBS) were procured from Invitrogen U.S.A.

The elemental analysis of the complexes was done using a Thermo Finnigan FLASH EA 1112 CHNS analyzer. The infrared and electronic spectra (UV-Vis) were recorded with Bruker Alpha and Perkin–Elmer spectrum one 55 spectrometers, respectively. Molar conductivity measurements were made with a Control Dynamics (India) conductivity meter. Electrochemical measurements were made with an EG&G PAR model 253 VersaStat potentiostat/galvanostat with electrochemical analysis software 270 using a three-electrode setup (glassy carbon working, platinum wire auxiliary and a saturated calomel reference electrode in DMF-0.1 M TBAP as the supporting electrolyte). Electrospray ionization (ESI) mass spectral measurements were made using an Agilent Technologies 6538 Ultra High definition accurate-mass Q-TOF LC/MS ESI model mass spectrometer. Fluorescence measurements at 25 °C were done using a Perkin–Elmer LS 55 fluorescence spectrometer. The fluorescence quantum yield values of the compounds were obtained by a relative method as described in the literature.[54] Flow cytometric analysis was carried out using FACS (fluorescence-activated cell sorting) Calibur Becton Dickinson (BD) cell analyzer at FL2 channel (595 nm). ICPMS study was performed in HeLa cells by using Quadrupole Inductively Coupled Plasma Mass Spectrometer (Thermo X Series II). Confocal microscopy images were acquired from Olympus FV 3000 inverted microscope with oil immersion lens of 60X and 100X magnification.

Synthesis of ligands: The ligands were prepared using reported protocols (Scheme S1).[55] D-Biotin (1.22 g, 1 eq.) was dissolved in 50 mL anhydrous DMF and stirred for 10 min to get a colorless solution. N-Hydroxy succinimide (0.58 g, 1 eq.) was added to the solution followed by addition of a catalytic amount of DCC (coupling agent). The solution was stirred at room temperature for 8 h to obtain the biotin-NHS ester. The solvent was evaporated to obtain a fluffy light-yellow powder (1.57 g). The ester was further dissolved in 40 mL DMF under nitrogen atmosphere and ethylene diamine (0.32 mL, 1 eq) was added dropwise to the mixture. A 0.3 mL triethylamine was added to the mixture and it was allowed to stir for 8 h at 50 °C. The solvent was reduced, and product was extracted with CH_2Cl_2 (5 × 20 mL) to obtain the precursor species. Refluxing 2 eq. of 2-picolyl chloride (0.7 mL) with the precursor (1 eq, 1 g) for 12 h in 40 ml DMF in the presence of 5 N NaOH yielded a green colored oil which was isolated after evaporation of the solvent. This oil was subjected to column chromatography and the final product eluted at 3:2 ethylacetate-CH_2Cl_2 in ~40% yield (0.65 g; MW: 468.6149). This NNN-biotin ligand L^2 was washed with ether to obtain a sticky solid, which becomes powdery upon drying under P_4O_{10} (M.P: 227 °C). The ligand was characterized by NMR, mass spectroscopy, and IR before using for metal complexation (Figures S1-S3, S5).

Synthesis of $[Fe(L^1/L^2)(cur)Cl]Cl$ (1 and 2): The complexes were synthesized following a general protocol wherein anhydrous $FeCl_3$ (1 eq, 0.16 g) was dissolved in 5 mL anhydrous methanol and 1 eq. of the dipicolylamine-based ligand [L^1 (0.24 g) for 1, L^2 (0.47 g) for 2] also dissolved in methanol was added drop-wise under a flow of nitrogen at 25 °C. This reaction mixture was allowed to stir for 2 h. A light brown colored intermediate of formulation $[Fe(L^1/L^2)Cl_3]$ was isolated and washed with hexane. One equivalent of the intermediate (0.4 g for 1, 0.63 g for 2) was dissolved in methanol. Curcumin (HCur, 1 eq. 0.37 g) was dissolved in 5 mL methanol and then deprotonated by treating with 1 eq. of triethylamine (0.1 g).

This solution was then added to the reaction mixture and stirred for 5 h. The solution was filtered, and slow evaporation of the solvent yielded a dark brown solid that was isolated and washed with ether and dried in vacuum over P_4O_{10}.

[Fe(L¹)(cur)Cl]Cl (1): Yield: 85% (0.62 g) $C_{35}H_{37}FeN_4O_6Cl_2$ (MW: 736.4425): calcd. C 57.08, H 5.06, N 7.61; found C 57.01, H 5.09, N 7.59. ESI-MS in CH_3CN calculated for $[M–Cl]^+$ (*m/z*): 700.1751; found: 700.2156 IR data: ν = 417 (w), 735 (m), 1160 (m), 1290 (s), 1500 (vs), 3075 (br) cm^{-1} (vs, very strong; s, strong; m, medium; w, weak; br, broad). UV/Vis (1:1 DMSO/DPBS): λ_{max}/nm [$\varepsilon/M^{-1}cm^{-1}$] = 437 [$3.25\times10^4$]. Molar conductivity in DMF at 298 K (Λ_M): 58 $S\,m^2\,M^{-1}$. μ_{eff} at 298 K: 5.83 μ_B.

[Fe(L²)(cur)Cl]Cl (2): Yield: 75% (0.7 g) $C_{45}H_{51}FeN_6O_8SCl_2$ (MW: 962.7378): calcd. C 56.14, H 5.34, N 8.73; found C 56.12, H 5.37, N 8.68. ESI-MS in CH_3CN calculated for $[M–Cl]^+$ (*m/z*): 926.2527; found: 926.2710 $[M–Cl]^+$. IR data: ν = 420 (w), 745 (m), 1080 (s), 1330 (vs), 1505 (s), 1590 (m), 3400 (br) cm^{-1}. UV/Vis (1:1 DMSO/DPBS): λ_{max}/nm [($\varepsilon/M^{-1}cm^{-1}$)] = 440 [$3.07\times10^4$], 450 (sh, shoulder) [$2.64\times10^4$]. Molar conductivity in DMF at 298 K (Λ_M): 63 $S\,m^2\,M^{-1}$. μ_{eff} at 298 K: 5.87 μ_B.

Theoretical Calculations

The geometries of the complexes 1 and 2 were optimized by density functional theory (DFT) using B3LYP level of theory and LanL2DZ basis set as implemented in Gaussian 09 program.[39] The electronic transitions with their transition probability were obtained using linear response time dependent density functional theory (TDDFT). The coordinates of the energy minimized structures and selected transitions in the visible region are listed in Table S1, Table S2 (vide Supporting Information). Some estimated bond distances and angles for the complexes **1** and **2** from the DFT calculations are given in Table S3 and Table S4 (vide Supporting Information).

Biological Experiments

HeLa, MCF-7 and HepG2 cells were grown in 100 mm polymer culture dishes (SPL Life sciences, Korea) in DMEM. The media was supplemented with 10% FBS, 100 U penicillin/mL, 100 μg streptomycin/mL and incubated in a humidified 5% CO_2 incubator (Sanyo, UK) at 37 °C. MTT assay was done to study the photocytotoxic behavior of the complexes in these cells using a broad-band visible light (400–700 nm) photoreactor (Luzchem Model LZC-1, Ontario, Canada; light fluence rate: 2.4 $mW\,cm^{-2}$; light dose: 10 $J\,cm^{-2}$). Approximately 8×10^3 cells were seeded for each of the cell line in two 96 well plates in 100 μL media per well. The cells were grown for 24 h at 37 °C in a CO_2 incubator. The complexes were dissolved in 2% DMSO and were added to the cells at different concentrations. Incubation was continued for another 4 h and then the media of one plate was replaced with DPBS and photo-irradiated for 1 h in broad-band visible light (400–700 nm). This was followed by removal of DPBS and addition of fresh media. The media of the other plate was discarded right after 4 h and replaced with fresh media. Both the plates were incubated further for 20 h in the dark. Then 25 μL MTT (4 $mg\,mL^{-1}$) was added in each well and incubated in dark for an additional 3 h. Finally, the culture media was discarded from each well of the plates and 200 μL DMSO was added to each well to solubilize the purple formazan crystals. Molecular Devices Spectra Max M5 plate reader was used to measure the absorbance at 540 nm. The cytotoxicity of the complexes was measured as the percentage ratio of absorbance of treated cells to the untreated controls. The IC_{50} values were determined by using nonlinear regression analysis (Graph Pad Prism 6). The experiment was repeated with cells that were pretreated with biotin (2 mM) 1 h prior to treatment with the complexes.

For cellular incorporation assay, ~0.4×10^6 cells/well were seeded in 12-well plates. Cells were allowed to grow undisturbed for 24 h. Subsequently, the cellular media was replaced by fresh media, complexes were added (2% DMSO) and incubated for 4 h. The cells were then washed with PBS and trypsinized. They were centrifuged to obtain cell pellets which were resuspended in 400 μL PBS. They were acquired on the BD FACS Verse™ flow cytometer (BD Biosciences, USA). Singlet gate (forward scatter-area versus forward scatter-height) and live gate (forward scatter-area versus side scatter-area) was used to select the viable cells and ~10,000 events were recorded. The analysis of results and construction of histograms was done using the flow cytometry analysis software, BD FACSDiva™.

The fluorogenic dye, 2′,7′-dichlorofluorescein diacetate (DCFDA) was used to measure the intracellular oxidative stress. In 12-well plates, the cells were seeded and incubated for 24 h. Subsequently, the cells were treated with the compounds for 4 h at 37 °C in dark. This was followed by 1 h visible light photo-irradiation during which DMEM was replaced by colourless saline buffer. Post exposure, the cells were washed, trypsinized and re-suspended in DPBS. Trypan blue exclusion assay was used to count viable cell numbers using a hemocytometer. About 0.25×10^6 viable cells were stained with 10 μM of DCFDA and incubated at 37 °C for 30 min in dark. The stain was then washed off and the cells were re-suspended in PBS. Data was acquired (1.0×10^4 cells in the live singlet gate) on the BD FACS Verse™ flow cytometer (BD Biosciences, USA). The results were analyzed and the representative histograms were constructed using the flow cytometry analysis software, BD FACSDiva™.

The cells were stained with Annexin V-FITC and PI to determine the mode of cell death. About 0.5×10^6 cells were seeded and incubated for 24 h in 6-well plates, post which, the cells were treated with the compounds for 4 h at 37 °C in dark. This was followed by 1 h photo-exposure. The cells were subsequently washed, trypsinized and re-suspended in PBS buffer. Viable cells were stained with Annexin V-FITC and PI in the binding buffer solution (APOAF, Sigma Aldrich) for 20 min. The cells were acquired (10000 events in the singlet gate) on the BD FACS Verse™ flow cytometer (BD Biosciences, USA). Construction of the Annexin V-FITC versus PI dot-plots, analysis, and quantification of the results was done using BD FACSDiva™ software.

Quantification of Cellular Iron by ICPMS

About 2×10^6 cells were seeded in complete culture medium supplemented with 10% heat-inactivated fetal bovine serum and maintained at 37 °C in a humidified atmosphere containing 5% CO_2. The complexes were added for final concentration of 15 μM and allowed to incubate for 4 h. After drug exposure, the cells were washed with DPBS solution. The wells were treated with 0.5 mL 65 °C nitric acid for 1.5 h and left to digest at room temperature. Afterwards, solutions were quantitatively transferred into 15 mL tubes and analysed by ICP-MS. The total iron content was calculated as ng/mL of protein or ppb.[57]

Confocal microscopy study

To study the cellular localization pattern of the fluorescent complex (20 μM) inside HeLa cells, confocal microscopy was used (Olympus FV 3000). ~0.5×10^5 cells were seeded in each glass bottom dish

(NunC, Thermofisher). Standard experimental procedures were adopted for processing them after treatment with the complexes.[58]

Co-localization study

To understand the sub-cellular localization of the complex, HeLa cells were incubated with 20 μM of complex 2 for 4 h in dark. After the incubation time, the medium was removed, and cells were washed thrice with DPBS. Nuclear staining dye Hoechst (1μL/1 mL) was added to the required wells for 8 min. Mito tracker red (250 nM)/Lyso tracker red (150 nM) was added to the cells and incubated for 30 min at room temperature. The cells were then directly observed under a confocal microscope (Olympus FV 3000) at 100X magnification.

Supporting Information (see footnote on the first page of this communication): General synthetic scheme of ligands and complexes (Scheme S1, S2), coordinates from DFT study (Table S1, Table S2), estimated bond distances and angles from DFT calculations (Table S3, Table S4), characterization of L^2 (Figures S1–S3, S6), ESI-MS spectra of complexes (Figures S4, S5), IR spectra (Figure S7), cyclic voltammograms (Figures S8, S9), photo-stability UV-Visible plots for complexes (Figure S10), photo-stability scatter plots for complexes and HCur with error bars (Figure S2), concentration vs. % cell viability MTT plots (Figures S13–S15), time dependent incorporation studies (Figure S16), effect of biotin pre-saturation on incorporation (Figure S17), co-localization studies with Mito tracker deep red and lysotracker deep red (Figure S18, S19), DNA binding MVH plots (Figure S20), and gel electrophoresis diagrams (Figures S21, S22),

Acknowledgements

We thank the Department of Science and Technology (DST), Government of India, for financial support (SR/S5/MBD-02/2007, EMR/2015/000742, CRG/2018/000081). A.R.C. thanks DST for J.C. Bose national fellowship (SR/S2/JCB-26/2007). We gratefully acknowledge the supports of the DBT-IISc partnership program, the bio-imaging and flow cytometry facility in the Division of Biological Sciences, IISc. We thank FACS operators and Puja from bioimaging facility in Biochemistry department. The authors thank the Alexander von Humboldt Foundation for donation of an electroanalytical system.

Conflict of Interest

The authors declare no conflict of interest.

Keywords: Iron · Curcumin · Biotin · Apoptosis · Antitumor agents

[1] a) F. Bray, J. Ferlay, I. Soerjomataram, R. L. Siegel, L. A. Torre, A. Jemal, *Ca-Cancer J. Clin.* **2018**, *68*, 394–424; b) B. W. Stewart, P. Kleihues, *World Cancer Report* (World Health Organization Press, Geneva, **2003**).
[2] P. E. Petersen, *Oral Oncol.* **2009**, *45*, 454–460.
[3] a) D. Evaluation, *Ther. Delivery* **2016**, *7*, 117–138; b) T. M. Allen, P. R. Cullis, *Science* **2004**, *303*, 1818–1822.
[4] J. Chalissery, D. Jalal, Z. Al-Natour, A. H. Hassan, *DNA Repair* **2017**, *51*, 2–13.
[5] M. Stucki, B. Pascucci, E. Parlanti, P. Fortini, S. H. Wilson, U. Hübscher, E. Dogliotti, *Oncogene* **1998**, *17*, 835–843.
[6] a) B. Ghazal, E. N. Kaya, A. Husain, A. Ganesan, M. Durmuş, S. Makhseed, *J. Porphyrins Phthalocyanines* **2019**, *23*, 46–55; b) R. Ackroyd, C. Kelty, N. Brown, M. Reed, *Photochem. Photobiol.* **2001**, *74*, 656–669.
[7] R. A. Craig, C. P. McCoy, S. P. Gorman, D. S. Jones, *Expert Opin. Drug Delivery* **2015**, *12*, 85–101.
[8] M. C. DeRosa, R. J. Crutchley, *Coord. Chem. Rev.* **2002**, *233–234*, 351–371.
[9] J. S. McCaughan Jr, *Drugs Aging* **1999**, *15*, 49–68.
[10] I. Diamond, A. F. Mcdonagh, C. B. Wilson, S. G. Granelli, S. Nielsen, R. Jaenicke, *The Lancet* **1972**, *300*, 1175–1177.
[11] S. I. Moriwaki, J. Misawa, Y. Yoshinari, I. Yamada, M. Takigawa, Y. Tokura, *Photodermatol. Photoimmunol. Photomed.* **2001**, *17*, 241–243.
[12] T. Nonaka, A. Nanashima, M. Nonaka, M. Uehara, H. Isomoto, Y. Nonaka, T. Nagayasu, *J. Hepatobiliary Pancreat Sci.* **2011**, *18*, 592–600.
[13] L. B. Josefsen, R. W. Boyle, *Met.-Based Drugs* **2008**, 1–24.
[14] A. K. Renfrew, *Metallomics* **2014**, *6*, 1324–1335.
[15] X. Wang, Z. Guo, *Chem. Soc. Rev.* **2013**, *42*, 202–224.
[16] C. Sawyers, *Nature* **2004**, *432*, 294–297.
[17] R. Spector, C. E. Johanson, *J. Neurochem.* **2007**, *103*, 425–438.
[18] T. Uppal, N. V. S. D. K. Bhupathiraju, M. G. H. Vicente, *Tetrahedron* **2013**, *69*, 4687–4693.
[19] D. Hanahan, R. A. Weinberg, *Cell* **2011**, *144*, 646–674.
[20] a) S. Chen, X. Zhao, J. Chen, J. Chen, L. Kuznetsova, S. S. Wong, I. Ojima, *Bioconjugate Chem.* **2010**, *21*, 979–987; b) M. W. Tibbitt, J. E. Dahlman, R. Langer, *J. Am. Chem. Soc.* **2016**, *138*, 704–717; c) D. S. Wilbur, M. K. Chyan, P. M. Pathare, D. K. Hamlin, M. B. Frownfelter, B. B. Kegley, *Bioconjugate Chem.* **2000**, *11*, 569–583; d) A. Baschieri, S. Muzzioli, V. Fiorini, E. Matteucci, M. Massi, L. Sambri, S. Stagni, *Organometallics* **2014**, *33*, 6154–6164; e) S. Y. S. Chow, S. Zhao, P.-C. Lo, D. K. P. Ng, *Dalton Trans.* **2017**, *46*, 11223–11229.
[21] U. Basu, I. Khan, A. Hussain, P. Kondaiah, A. R. Chakravarty, *Angew. Chem. Int. Ed.* **2012**, *51*, 2658–2661; *Angew. Chem.* **2012**, *124*, 2712–2715.
[22] S. Saha, R. Majumdar, M. Roy, R. R. Dighe, A. R. Chakravarty, *Inorg. Chem.* **2009**, *48*, 2652–2663.
[23] A. Garai, U. Basu, I. Khan, I. Pant, A. Hussain, P. Kondaiah, A. R. Chakravarty, *Polyhedron* **2014**, *73*, 124–132.
[24] A. Jana, B. K. Verma, A. Garai, P. Kondaiah, A. R. Chakravarty, *Inorg. Chim. Acta* **2018**, *483*, 571–578.
[25] a) T. Choudhuri, S. Pal, T. Das, G. Sa, *J. Biol. Chem.* **2005**, *280*, 20059–20068; b) T. Esatbeyoglu, P. Huebbe, I. M. A. Ernst, D. Chin, A. E. Wagner, G. Rimbach, *Angew. Chem. Int. Ed.* **2012**, *51*, 5308–5332; *Angew. Chem.* **2012**, *124*, 5402–5427; c) N. R. Jana, P. Dikshit, A. Goswami, N. Nukina, *J. Biol. Chem.* **2004**, *279*, 11680–11685.
[26] S. Banerjee, A. R. Chakravarty, *Acc. Chem. Res.* **2015**, *48*, 2075–2083.
[27] a) A. K. Chakravarty, S. N. Chatterjee, H. Yasmin, T. Mazumder, *Int. J. Pharmacol.* **2009**, *5*, 333–345; b) G. Padmanaban, V. A. Nagaraj, *ACS Med. Chem. Lett.* **2017**, *8*, 274–274; c) K. M. Nelson, J. L. Dahlin, J. Bisson, J. Graham, G. F. Pauli, M. A. Walters, *J. Med. Chem.* **2017**, *60*, 1620–1637; d) J. B. Baell, *J. Nat. Prod.* **2016**, *79*, 616–628.
[28] D. Pucci, A. Crispini, B. Sanz Mendiguchía, S. Pirillo, M. Ghedini, S. Morelli, L. De Bartolo, *Dalton Trans.* **2013**, *42*, 9679–9687.
[29] A. Garai, I. Pant, S. Banerjee, B. Banik, P. Kondaiah, A. R. Chakravarty, *Inorg. Chem.* **2016**, *55*, 6027–6035.
[30] R. Pettinari, F. Marchetti, F. Condello, C. Pettinari, G. Lupidi, R. Scopelliti, S. Mukhopadhyay, T. Riedel, P. J. Dyson, *Organometallics* **2014**, *33*, 3709–3715.
[31] P. Prasad, I. Pant, I. Khan, P. Kondaiah, A. R. Chakravarty, *Eur. J. Inorg. Chem.* **2014**, 2420–2431.
[32] K. Mitra, S. Gautam, P. Kondaiah, A. R. Chakravarty, *Angew. Chem. Int. Ed.* **2015**, *54*, 13989–13993; *Angew. Chem.* **2015**, *127*, 14195–14199.
[33] B. Banik, K. Somyajit, G. Nagaraju, A. R. Chakravarty, *Dalton Trans.* **2014**, *43*, 13358–13369.
[34] A. Hussain, K. Somyajit, B. Banik, S. Banerjee, G. Nagaraju, A. R. Chakravarty, *Dalton Trans.* **2013**, *42*, 182–195.
[35] a) R. M. Burger, *Chem. Rev.* **1998**, *98*, 1153–1169; b) U. Basu, M. Roy, A. R. Chakravarty, *Coord. Chem. Rev.* **2020**, *417*, 213339; c) M. Bouché, C. Hognon, S. Grandemange, A. Monari, P. C. Gros, *Dalton Trans.* **2020**, *49*, 11451–11466.
[36] K. Nakamato, *Infrared and Raman Spectra of Inorganic and Coordination Compounds*, John Wiley and Sons: New York, **1997**.
[37] K. I. Priyadarsini, *Molecules* **2014**, *19*, 20091–20112.
[38] R. M. Burger, S. J. Projan, S. B. Horwitz, J. Peisach, *J. Biol. Chem.* **1986**, *261*, 15955–15959.

[39] A. Bhattacharyya, A. Dixit, K. Mitra, S. Banerjee, A. A. Karande, A. R. Chakravarty, *MedChemComm* **2015**, *6*, 846–851.
[40] a) A. D. Becke, *Phys. Rev. A* **1988**, *38*, 3098–3100; b) W. R. Wadt, P. J. Hay, *J. Chem. Phys.* **1985**, *82*, 284–298; c) M. J. Frisch, G. W. Trucks, H. B. Schlegel, G. E. Scuseria, M. A. Robb, J. R. Cheeseman, G. Scalmani, V. Barone, B. Mennucci, G. A. Petersson, H. Nakatsuji, M. Caricato, X. Li, H. P. Hratchian, A. F. Izmaylov, J. Bloino, G. Zheng, J. L. Sonnenberg, M. Hada, M. Ehara, K. Toyota, R. Fukuda, J. Hasegawa, M. Ishida, T. Nakajima, Y. Honda, O. Kitao, H. Nakai, T. Vreven, J. A. Montgomery Jr., J. E. Peralta, F. Ogliaro, M. Bearpark, J. J. Heyd, E. Brothers, K. N. Kudin, V. N. Staroverov, R. Kobayashi, J. Normand, K. Raghavachari, A. Rendell, J. C. Burant, S. S. Iyengar, J. Tomasi, M. Cossi, N. Rega, J. M. Millam, M. Klene, J. E. Knox, J. B. Cross, V. Bakken, C. Adamo, J. Jaramillo, R. Gomperts, R. E. Stratmann, O. Yazyev, A. J. Austin, R. Cammi, C. Pomelli, J. W. Ochterski, R. L. Martin, K. Morokuma, V. G. Zakrzewski, G. A. Voth, P. Salvador, J. J. Dannenberg, S. Dapprich, A. D. Daniels, Ö. Farkas, J. B. Foresman, J. V. Ortiz, J. Cioslowski, D. J. Fox, *Gaussian 09*, *Revision A.02*, *Gaussian*, *Inc.*, *Wallingford CT*, **2009**.
[41] S. Banerjee, P. Prasad, A. Hussain, I. Khan, P. Kondaiah, A. R. Chakravarty, *Chem. Commun.* **2012**, *48*, 7702–7704.
[42] T. K. Goswami, S. Gadadhar, B. Gole, A. A. Karande, A. R. Chakravarty, *Eur. J. Med. Chem.* **2013**, *63*, 800–810.
[43] E. Delaey, F. Van Laar, D. De Vos, A. Kamuhabwa, P. Jacobs, P. De Witte, *Photochem. Photobiol. B* **2000**, *55*, 27–36.
[44] a) S. Saha, R. Majumdar, A. Hussain, R. R. Dighe, A. R. Chakravarty, *Philos. Trans. R. Soc. London Ser. A* **2013**, *371*, 20120190; b) K. Mitra, U. Basu, I. Khan, B. Maity, P. Kondaiah, A. R. Chakravarty, *Dalton Trans.* **2014**, *43*, 751–763.
[45] T. Sarkar, A. Hussain, *Enzyme Eng.* **2016**, *5*, 1–6.
[46] A. P. Demchenko, *Exp. Oncol.* **2012**, *34*, 263–268.
[47] T. Takanashi, Y. Ogura, H. Taguchi, M. Hashizoe, Y. Honda, *Invest. Ophthalmol. Visual Sci.* **1997**, *38*, 2721–2728.
[48] a) J. D. McGhee, P. H. Von Hippel, *J. Mol. Biol.* **1974**, *86*, 469–489; b) M. T. Carter, M. Rodriguez, A. J. Bard, *J. Am. Chem. Soc.* **1989**, *111*, 8901–8911.
[49] J. De Laat, H. Gallard, *Environ. Sci. Technol.* **1999**, *33*, 2726–2732.
[50] a) C. J. Burrows, J. G. Muller, *Chem. Rev.* **1998**, *98*, 1109–1152; b) K. Szacilowski, W. Macyk, A. Drzewiecka-Matuszek, M. Brindell, G. Stochel, *Chem. Rev.* **2005**, *105*, 2647–2694.
[51] M. Athar, H. Mukhtar, D. R. Bickers, *J. Invest. Dermatol.* **1988**, *90*, 652–657.
[52] J. P. Kehrer, *Toxicology* **2000**, *149*, 43–50.
[53] D. D. Perrin, W. L. F. Armarego, D. R. Perrin, *Purification of Laboratory Chemicals*, Pergamon Press, Oxford, **1980**.
[54] a) A. P. Thomas, P. S. S. Babu, S. A. Nair, S. Ramakrishnan, D. Ramaiah, T. K. Chandrashekar, A. Srinivasan, M. R. Pillai, *J. Med. Chem.* **2012**, *55*, 5110–5120; b) A. T. R. Williams, S. A. Winfield, J. N. Miller, *Analyst* **1983**, *108*, 1067–1071.
[55] a) S. James, K. P. Maresca, D. G. Allis, J. F. Valliant, W. Eckelman, J. W. Babich, J. Zubieta, *Bioconjugate Chem.* **2006**, *17*, 579–589; b) X. Jiang, M. Ahmed, Z. Deng, R. Narain, *Bioconjugate Chem.* **2009**, *20*, 994–1001; c) J. Li, L. Zeng, K. Xiong, T. W. Rees, C. Jin, W. Wu, Y. Chen, L. Ji, H. Chao, *Chem. Commun.* **2019**, *55*, 10972–10975.
[56] a) L. A. Herzenberg, J. Tung, W. A. Moore, L. A. Herzenberg, D. R. Parks, *Nat. Immunol.* **2006**, *7*, 681–685; b) D. R. Parks, M. Roederer, W. A. Moore, *Cytometry Part A* **2006**, *69*, 541–551.
[57] a) M. Hedayati, O. Thomas, B. Sharif, H. Zhou, C. Cornejo, Y. Zhang, M. Wabler, J. Mihalic, C. Gruettner, F. Westphal, A. Geyh, T. Deweese, R. Ivkov, *Nanomedicine* **2013**, *8*, 29–41; b) A. E. Egger, C. Rappel, M. A. Jakupec, C. G. Hartinger, P. Heffeter, B. K. Keppler, *J. Anal. At. Spectrom.* **2009**, *24*, 51–61.
[58] a) J. L. McClintock, B. P. Ceresa, *Invest. Ophthalmol. Visual Sci.* **2010**, *51*, 3455–3461; b) D. Semwogerere, E. R. Weeks, *Encycl. Biomater. Biomed. Eng.* **2005**, 1–10.

Manuscript received: December 30, 2020
Revised manuscript received: March 16, 2021
Accepted manuscript online: March 20, 2021